

# Toward New Thermoelectrics: Tin Selenide/Modified Graphene Oxide Nanocomposites

Iryna S. Protsak,<sup>†,‡</sup> Simon Champet,<sup>†</sup> Chang-Yang Chiang,<sup>‡</sup> Wuzong Zhou,<sup>‡,§</sup> Srinivas R. Popuri,<sup>§</sup> Jan-Willem G. Bos,<sup>§</sup> Dinesh K. Misra,<sup>||</sup> Yevhenii M. Morozov,<sup>⊥,¶</sup> and Duncan H. Gregory<sup>\*,†,§</sup>

<sup>†</sup>WestCHEM, School of Chemistry, University of Glasgow, Glasgow G12 8QQ, U.K.

<sup>‡</sup>EaSTCHEM, School of Chemistry, University of St Andrews, St Andrews, Fife KY 16 9ST, U.K.

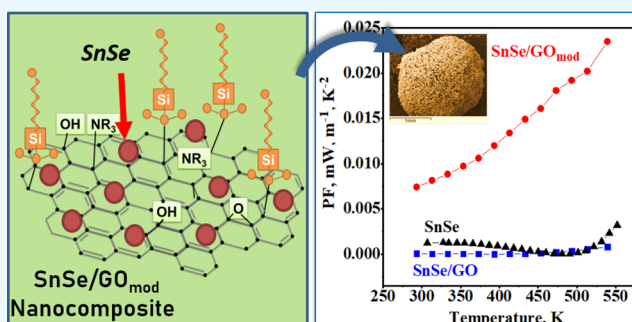
<sup>§</sup>Institute of Chemical Sciences and Centre for Advanced Energy Storage and Recovery, School of Engineering and Physical Sciences, Heriot-Watt University, Edinburgh EH14 4AS, U.K.

<sup>||</sup>CSIR-National Physical Laboratory, Dr. K.S. Krishnan Marg, New Delhi 110012, India

<sup>⊥</sup>Institute for Information Recording of NASU, 2 Shpaka Street, Kiev 03113, Ukraine

## Supporting Information

**ABSTRACT:** New nanocomposites have been prepared by combining tin selenide (SnSe) with graphene oxide (GO) in a simple aqueous solution process followed by ice templating (freeze casting). The resulting integration of SnSe within the GO matrix leads to modifications of electrical transport properties and the possibility of influencing the power factor ( $S^2\sigma$ ). Moreover, these transport properties can then be further improved ( $S$ ,  $\sigma$  increased) by functionalization of the GO surface to form modified nanocomposites (SnSe/GO<sub>mod</sub>) with enhanced power factors in comparison to unmodified nanocomposites (SnSe/GO) and “bare” SnSe itself. Functionalizing the GO by reaction with octadecyltrimethoxysilane (C<sub>21</sub>H<sub>46</sub>O<sub>3</sub>Si) and triethylamine ((CH<sub>3</sub>CH<sub>2</sub>)<sub>3</sub>N) switches SnSe from p-type to n-type conductivity with an appreciable Seebeck coefficient and high electrical conductivity (1257 S·m<sup>-1</sup> at 539 K), yielding a 20-fold increase in the power factor compared to SnSe itself, prepared by the same route. These findings present new possibilities to design inexpensive and porous nanocomposites based on metal chalcogenides and functionalized carbon-derived matrices.



## 1. INTRODUCTION

Sustainable means of energy storage and conversion are vital globally, given the economic, security, and environmental concerns associated with fossil fuels. There is an urgent need to consume less power and improve energy efficiency. Thermoelectric materials have been studied for many years and offer a very convenient method of converting waste heat into useful power. However, the efficiency of this process is too low to be cost-effective.<sup>1,2</sup>

The conversion efficiency of thermoelectric materials is determined by the figure of merit,<sup>3</sup>  $ZT = S^2\sigma T/\kappa$ , where  $\sigma$  is the electrical conductivity,  $S$  is the Seebeck coefficient,  $T$  is the temperature, and  $\kappa$  is the thermal conductivity. To maximize the  $ZT$  value, a high Seebeck coefficient is required, coupled with small thermal conductivity and high electrical conductivity. Nanostructuring can very effectively enhance  $ZT$ , where most notably the high density of interfaces can improve phonon scattering, decreasing the lattice thermal conductivity.

Tin selenide (SnSe) is a narrow band gap, binary IV–VI semiconductor, suitable for various optoelectronic applications like memory switching devices, photovoltaics, and light emitting devices. It has also emerged as a highly promising

thermoelectric material over the last 4 years.<sup>4</sup> SnSe is characterized by excellent energy conversion efficiency, low cost, and high earth abundance of the component elements.<sup>5–10</sup> Most current research has been concentrated mainly on p-type SnSe<sup>11–15</sup> and conversely n-type SnSe<sup>16–18</sup> is more difficult to achieve. The high efficiency of SnSe as a thermoelectric material is determined to a great extent by the method of its production. To synthesize SnSe with appreciable  $ZT$  values, the use of toxic chemicals, high annealing temperatures, and long processing times is required. Alternative solution-based syntheses can be used to produce nanostructured SnSe in bulk quantities under much milder and simpler conditions, but use of surfactants to control growth and morphology can lead to relatively meagre thermoelectric properties.<sup>19</sup>

Recently, graphene-based materials have been explored for their potential as thermoelectrics.<sup>20,21</sup> With appropriate nanostructuring and band gap engineering, studies have

Received: November 11, 2018

Accepted: February 28, 2019

Published: March 29, 2019

demonstrated that both the lattice thermal conductivity of carbon derivatives can be reduced and the Seebeck coefficient can be enhanced without dramatically decreasing electrical conductivity.<sup>22</sup> Various graphene nanostructures have thus been predicted to possess *ZT* values sufficient to make them attractive for energy conversion.<sup>22</sup> Similarly, the chemical modification of the graphene or graphene oxide (GO) surface provides alternative routes to engineer the mechanical, electrical, and thermal properties. For instance, experiments show that aromatic molecules tethered to graphene layers can increase the power factor by a factor of 8 compared to that of an unmodified graphene film.<sup>23</sup> Carbon is light, abundant, relatively cheap, and easily recyclable and so it presents a number of other attractions in terms of a potential thermoelectric.<sup>24</sup> However, neither pure graphene nor GO have yet demonstrated a superior thermoelectric performance experimentally.

The best examples of SnSe thermoelectric performance arise in large, dense single crystals, whereas bulk powders (especially, some of those synthesized under mild conditions) can often exhibit relatively mediocre *ZT* values compared to such crystals. Emerging studies over the last 5 years have begun to demonstrate that graphene and its derivatives can be used effectively as a component in composite materials, where either graphene is added in small concentrations to influence the grain boundaries or is employed to “wrap” nanoparticles of the active thermoelectric material. Examples in Bi<sub>2</sub>Te<sub>3</sub>, PbTe, and skutterudite systems demonstrate that charge carrier concentrations can be increased, the nature of the charge carriers altered (as manifested in a change of the sign of Seebeck coefficients), and thermal properties improved by increased phonon scattering at defects and grain boundaries.<sup>25–27</sup> Given the need to improve the thermoelectric properties of bulk SnSe and given the chemical flexibility associated with functionalizing carbons, an interesting alternative approach could thus be to engineer nanoscale composites comprising the selenide and modified GO. Although there are some reports of the application of types of SnSe/GO-based composite materials in photodetectors,<sup>28,29</sup> photocatalytic devices,<sup>30</sup> and sodium-ion batteries,<sup>31</sup> to the best of our knowledge, there are no existing reports of SnSe/GO-hierarchical nanocomposite materials or of using SnSe/GO composites for thermoelectric applications.

In this work, we demonstrate how it is possible to make SnSe nanocomposites with GO as a “host” matrix. The materials can be produced in bulk quantities and potentially cast into bespoke, well-defined, shaped, and sized monoliths. Additionally, we show that chemically modifying (functionalizing) the surface structure of the GO component is an effective way to manipulate the thermoelectric properties of the SnSe/GO nanocomposites. The rationale behind the functionalization of the GO component was first to modify the surface chemically with amine groups in aqueous media to produce hydroxyl groups, which act as electron donors and second to expand the interlayer distance between GO layers (using octadecyltriethoxysilane), thus preventing agglomeration and creating local structural disorder at the GO surface. Subsequent experiments show that both the electrical conductivity and Seebeck coefficient of the nanocomposites are influenced by functionalization. This approach suggests a new direction for modifying the thermoelectric performance of chalcogenides and lays the foundations for the design of other kinds of GO-based thermoelectric composites.

## 2. EXPERIMENTAL SECTION

**2.1. Synthesis of GO.** GO nanosheets were prepared by the improved Hummers' method.<sup>32,33</sup> In detail, a 9:1 mixture of concentrated H<sub>2</sub>SO<sub>4</sub>/H<sub>3</sub>PO<sub>4</sub> (360:40 mL; analytical reagent grade, Fisher and 85% aq, Alfa-Aesar, respectively) was added to a mixture of graphene flakes (3.0 g; graphene nanoplatelet aggregates, Alfa-Aesar) and KMnO<sub>4</sub> (18.0 g; ACS reagent >99.0%, Sigma-Aldrich), in a mildly exothermic process at 40 °C. The mixture was subsequently heated to 50 °C and stirred for 16 h before cooling with ice and water (400 mL). Once cooled, 30% of H<sub>2</sub>O<sub>2</sub> (7 mL; 30%, VWR) was added slowly to the reaction mixture, which was subsequently stirred for 5–6 h until the mixture color changed from light yellow to brown. The product was washed with deionized (DI) water to remove any oxidant residues entirely. The resulting solution was poured into 40 mL centrifuge tubes and centrifuged for 1 h at 4000 rpm before separating the oxidant residues to yield a brown solid. The process was repeated more than 10 times until the product was thoroughly washed. For the preparation of GO dispersions, the solid products were redispersed in DI and sonicated for 1 h at 200 W. The dispersions were purified by centrifugation for 20 min, and the upper half of their volume was selected for further studies.

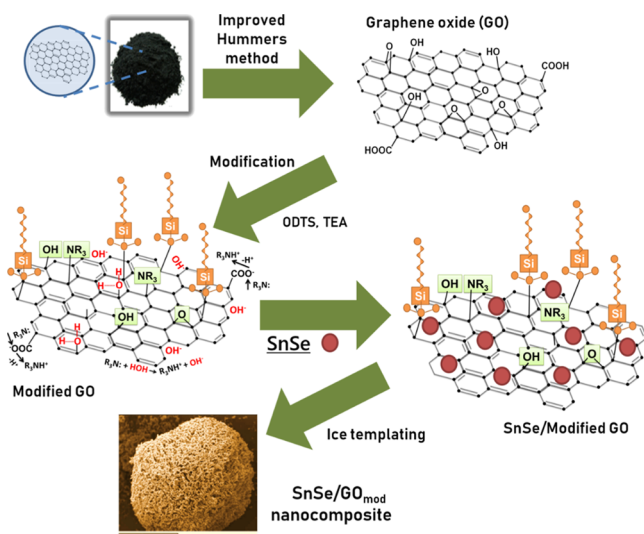
**2.2. Synthesis of SnSe Nanoparticles.** SnSe nanoparticles were synthesized via a citric acid-assisted solution synthesis,<sup>19</sup> which includes three steps: first, 285 mmol citric acid (99.5%, Alfa-Aesar) and 10 mmol SnCl<sub>2</sub>·2H<sub>2</sub>O (99.99%, Sigma-Aldrich) were dissolved in 50 mL of DI in a two neck round-bottom flask, so as to prepare a transparent solution containing Sn<sup>2+</sup> ions. Separately, 10 mmol Se (>99.5%, Sigma-Aldrich) and 23 mmol NaBH<sub>4</sub> (98%, Alfa-Aesar) were dissolved in 50 mL of DI in a single-neck round-bottom flask to prepare sodium hydrogen selenide (sodium biselenide; NaHSe). In the final stage, NaHSe was injected into the solution of Sn<sup>2+</sup> ions, which leads to the direct formation of a black precipitate of SnSe. The mixture was held at room temperature under Ar (99.998%, BOC) on a Schlenk line. The product was washed with DI and ethanol several times. The as-synthesized samples used for characterization and performance evaluation were stored in an Ar-filled MBraun glovebox (<0.5 ppm H<sub>2</sub>O, <0.5 ppm O<sub>2</sub>) to avoid possible reaction with air or water.

**2.3. Chemical Modification of GO.** As-synthesized GO was silylated following a procedure similar to that reported for the silylation of a layered silicate.<sup>34–37</sup> First, GO (160 mg) was mixed with toluene (20 mL; 99%, Alfa-Aesar), and the mixture was sonicated for 1 h under a nitrogen atmosphere to form a homogeneous solution. Octadecyltrimethoxysilane (2 mL) (ODTS; C<sub>21</sub>H<sub>46</sub>O<sub>3</sub>Si; 98% Alfa-Aesar) was added slowly to the GO solution. Triethylamine (2 mL) (TEA; (CH<sub>3</sub>CH<sub>2</sub>)<sub>3</sub>N; 99.5%, Sigma-Aldrich) was injected into the reaction mixture, which was allowed to stand for 12 h. After 12 h at 50 °C, the product was washed and centrifuged with ethanol several times.

**2.4. Ice-Templating Synthesis of SnSe/GO Nanocomposites.** A modified ice-templating method was utilized to prepare SnSe/GO and SnSe/GO<sub>mod</sub> nanocomposites.<sup>34,38</sup> First, an aqueous solution of SnSe (2.2 g in 100 mL H<sub>2</sub>O) was mixed with an aqueous dispersion of GO (200 mg in 30 mL H<sub>2</sub>O) in 100 mL of distilled water and the mixture was sonicated for 1 h. The sonicated dispersion (100 mL) of nanoparticles was dropped slowly into a Dewar of liquid

nitrogen (600 mL) using a syringe equipped with a needle. Freezing lasted for 30 min until the suspension was completely frozen and brown, sponge-like, misshapen beads of SnSe/GO (with a size of ca. 1.5 mm × 1.5 mm × 2 mm; Scheme 1) were

### Scheme 1. Synthesis Steps for SnSe/GO<sub>mod</sub> Nanocomposites



formed. The SnSe/GO spheres were freeze-dried (Schlenk line at ca.  $3 \times 10^{-1}$  mbar and  $-196$  °C to ambient temperature) and dried further under vacuum overnight (16 h). The SnSe/GO<sub>mod</sub> nanocomposite was prepared following the same procedure described above for SnSe/GO and by way of example, the overall synthesis procedure for the SnSe/GO<sub>mod</sub> nanocomposite is shown in Scheme 1 (and in more detail in Scheme S1 in the Supporting Information). The modified and unmodified nanocomposites used for characterization and property measurements were stored in an Ar-filled MBraun glovebox ( $<0.5$  ppm H<sub>2</sub>O,  $<0.5$  ppm O<sub>2</sub>) to avoid any possible reaction with air or water.

**2.5. Materials Characterization.** Powder X-ray diffraction (XRD) patterns were recorded using a PANalytical X'pert Pro MPD diffractometer in Bragg–Brentano geometry (Cu K $\alpha_1$  radiation,  $\lambda = 1.5406$  Å). Diffraction data were typically collected in the angular range of  $2\theta = 5^\circ$ – $60^\circ$  for up to 12 h. Fourier transform infra-red (FTIR) spectroscopy was performed with a Jasco 4100 FTIR spectrometer operating in the 400–4000 cm<sup>-1</sup> spectral range to obtain FTIR spectra at room temperature. Raman spectroscopy was conducted using a LabRAM HR system (Horiba Jobin Yvon) with a Ventus 532 laser system operating at 100 mW and 532 nm.

The morphological and structural characteristics of the synthesized products were investigated by scanning electron microscopy (SEM) using a Carl Zeiss Sigma microscope equipped with an energy-dispersive X-ray spectrometer (Oxford Instruments X-Max 80), with accelerating voltages of 5 and 20 kV for imaging and energy-dispersive X-ray spectroscopy (EDS), respectively. The obtained nanocomposites were dispersed on a conductive carbon tape attached to a standard aluminium SEM sample stub.

The microstructure and crystallography were further investigated by high-resolution transmission electron microscopy (HRTEM) and selected area electron diffraction (SAED) using a JEOL 2011 microscope operated at 200 kV. TEM samples were prepared by mixing/grinding either SnSe or

nanocomposite (SnSe/GO) powders with acetone in an agate mortar. Three to six drops of the resulting suspension were dropped onto a 3 mm diameter holey C-coated Cu TEM grid.

**2.6. Measurement of the Electrical and Thermal Transport Properties of SnSe/GO Nanocomposites.** To measure the performance of the nanocomposites, the samples were loaded into a graphite die and hot-pressed into pellets at 500 °C for 20 min under Ar protection with a uniaxial pressure of  $\approx 60$  MPa. XRD data (see Supporting Information) and EDS spectra revealed no significant changes to the composition of the samples following hot pressing. The obtained pellets were cut into bars of dimensions 12 mm × 3 mm × 2 mm, and the Seebeck coefficient and electrical conductivity of the samples were measured perpendicular to the hot pressing direction using a Linseis LSR-3 instrument under a helium atmosphere over a temperature range of 290–540 K. The uncertainty in the measurement of the Seebeck coefficient and electrical conductivity is 5%. Electrical measurements were also performed on samples of SnSe itself (i.e., without addition of GO or modified GO), prepared by a similar process, for the purposes of comparison.

The total thermal conductivity was calculated through  $\kappa_{\text{tot}} = DC_p\rho$ , where  $D$  (the thermal diffusivity) was measured using a Linseis LFA 1000 instrument under vacuum conditions, over a temperature range of 290–540 K,  $C_p$  (the specific heat) was obtained via DSC measurements (822e Mettler Toledo), and  $\rho$  (the density) was determined from the sample mass and geometry. Lattice thermal conductivity ( $\kappa_{\text{lat}}$ ) was calculated via the Wiedemann–Franz law,  $\kappa = \kappa_{\text{tot}} - L\sigma T$ , where  $\kappa_{\text{tot}}$  is the total thermal conductivity,  $L$  is the Lorenz number,  $T$  is the temperature, and  $\sigma$  is the electrical conductivity.

### 3. RESULTS AND DISCUSSION

FTIR analysis gives valuable information about the presence of different chemical groups on the surface and was used both to confirm the degree of oxidation of GO and to monitor the passage of surface reactions after the modification of the GO surface. Figure 1 shows the FTIR spectra of (a) pristine GO and (b) silylated GO over the range of 500–4000 cm<sup>-1</sup>. For the pristine GO sample (Figure 1a), characteristic bands are observed at 822 and 1080–1331 cm<sup>-1</sup> (alkoxy C–O stretching and epoxy C–O–C stretching vibrations), 1723 cm<sup>-1</sup> (C=O stretching vibrations of COOH groups), 3450 and 1610 cm<sup>-1</sup> (stretching vibrations of hydrogen-bonded-OH group and

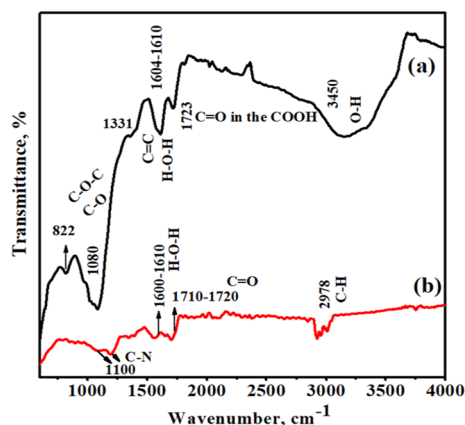


**Figure 1.** FTIR spectra of (a) pristine (untreated) and (b) modified (silylated) GO (GO<sub>mod</sub>).



adsorbed water), and  $1604\text{ cm}^{-1}$  (stretching vibrations of the  $\text{sp}^2$ -hybridized  $\text{C}=\text{C}$  bond in phenolic group).<sup>39</sup> By contrast, the IR spectra of modified GO (Figure 1b) show a reduction in the intensity of peaks assigned to the epoxy  $\text{C}-\text{O}-\text{C}$  stretching vibration in parallel with the appearance of new peaks at ca.  $1100$  and  $2978\text{ cm}^{-1}$ . These can be assigned to the  $\text{C}-\text{N}$  stretching vibration and to the  $\text{C}-\text{H}$  stretching vibration in alkyl groups, respectively, which may suggest that amine reacts with the epoxy groups at the GO surface by ring-opening reaction to generate  $\text{C}-\text{N}$  bonds. Additionally, the modified GO spectrum shows the disappearance of the hydroxyl group vibration at approximately  $3450\text{ cm}^{-1}$ , an intensity reduction in the peak due to adsorbed water at  $1600$ – $1610\text{ cm}^{-1}$  and the appearance of an alkyl band ( $2978\text{ cm}^{-1}$ ). All these features suggest that silane grafting occurs at the GO surface.

Raman spectroscopy is one of the most powerful tools to characterize the structure, bonding, level of disorder, and composition of carbon-based materials.<sup>40</sup> Figure 2 depicts the

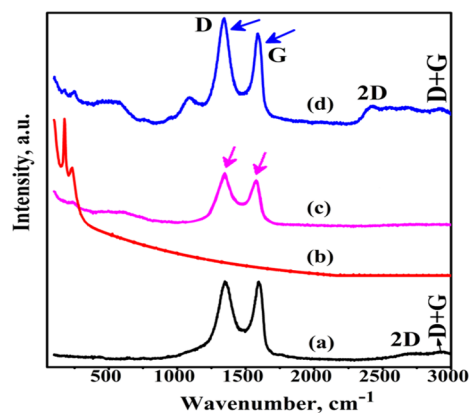


**Figure 2.** Raman spectra of (a) neat GO, (b) neat SnSe, (c) SnSe/GO nanocomposite, and (d) SnSe/GO<sub>mod</sub>.

Raman spectra of GO, SnSe, SnSe/GO, and SnSe/GO<sub>mod</sub>. The Raman spectra of GO (Figure 2a) show two prominent peaks at ca.  $1348$  and  $1597\text{ cm}^{-1}$ . The G band ( $1597\text{ cm}^{-1}$ ) belongs to the stretching of the  $\text{C}-\text{C}$  bond in graphitic materials and is common to all  $\text{sp}^2$  carbon systems. Meanwhile, the D band ( $1348\text{ cm}^{-1}$ ) is associated with the disordered structure of GO or structural defects.<sup>41</sup> The Raman spectra of pristine SnSe (Figure 2b) show a peak at  $150$ – $170\text{ cm}^{-1}$ , which originates from the  $A_{g1}$  vibration mode characteristic of the orthorhombic phase of SnSe.<sup>42</sup> The relative intensity of the D band is larger than that of the G band in the SnSe/GO<sub>mod</sub> (Figure 2d,  $I_D/I_G = 1.07$ ) nanocomposite as compared to GO itself (Figure 2a) as a consequence of the structural disorder induced by the modification of the GO. The higher intensity of the D-band can also be attributed to the alkyl groups which are anchored to the GO surface as the result of the silylation process (as manifested by  $\text{C}-\text{H}$  bands in the IR spectra; Figure 1b). Also, notable in the spectra is the presence of the 2D band at ca.  $2700\text{ cm}^{-1}$  (Figure 2a,d) that signifies the multilayer nature of the GO material, while the peak at ca.  $2940\text{ cm}^{-1}$  (Figure 2a,d) can be assigned to the combination mode of G and D bands (D + G band).<sup>43,44</sup> By comparison, considering the main features of the unmodified nanocomposite (SnSe/Ge; Figure 2d), the intensity of the D band (at  $1348\text{ cm}^{-1}$ ) is relatively only slightly higher than that of the G band (at  $1597\text{ cm}^{-1}$ )

( $I_D/I_G = 1.03$ ) but nonetheless indicates increased formation of structural defects compared to GO itself. The  $A_{g1}$  vibration band with a relatively weak intensity at  $150$ – $170\text{ cm}^{-1}$  from SnSe is observed as might be expected in the spectra of both nanocomposites (Figure 2c,d).

Figure 3 depicts XRD patterns of the components GO and SnSe and of the composites SnSe/GO and SnSe/GO<sub>mod</sub>. The

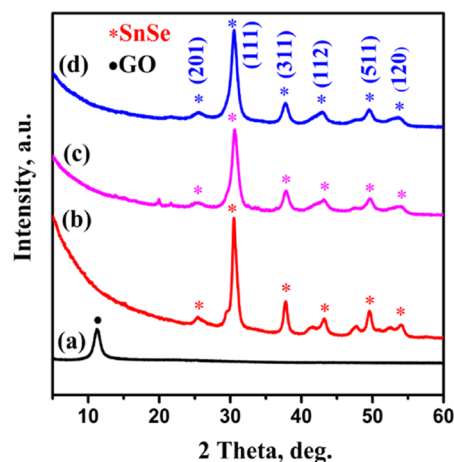


**Figure 3.** XRD patterns of (a) neat GO; (b) SnSe; (c) SnSe/GO, and (d) SnSe/GO<sub>mod</sub> (reflections marked with an asterisk and a dot correspond to those of SnSe and GO, respectively).

XRD pattern of GO contains one peak at  $10.5^\circ$ , which can be assigned to the (001) reflection with a corresponding interlayer distance of  $0.84\text{ nm}$  (Figure 3a). The relatively simple pattern is characteristic of GO and is consistent with a well-ordered GO structure that is sustained by the presence of water and different oxygen-containing functional groups,<sup>45</sup> such as those identified in the IR data presented above. The XRD pattern of pristine SnSe (Figure 3b) indicates the presence of the expected peaks corresponding to the most prominent reflections of the orthorhombic phase of SnSe. The diffraction pattern of the SnSe nanoparticles could be matched well to JCPDS-ICCD, card no. 32-1382, and all reflections could be indexed to the orthorhombic phase of SnSe.<sup>46–48</sup> No peaks indicative of Se,  $\text{SnO}_2$ ,  $\text{SnSe}_2$ , or any other impurities were present, and the SnSe samples were thus single-phase. The SnSe/GO and SnSe/GO<sub>mod</sub> nanocomposites (Figure 3c,d and S1) exhibit similar XRD patterns dominated by the SnSe phase reflections, with the notable observation that the peaks are considerably broader than those from the pristine sample of SnSe. The broadening of these reflections in the patterns of both nanocomposites likely reflects a reduction in the particle size compared to SnSe itself and indeed electron microscopy (HRTEM and SEM) corroborates this assumption and is discussed in more detail below.

Figure 4 shows SEM images of pristine SnSe and of both nanocomposites (SnSe/GO and SnSe/GO<sub>mod</sub>). Treatment of the SEM image (Figure 4c–e) using the ImageJ software with the Granulometry Plugin (based on grey level mathematical morphology operations)<sup>49</sup> allows us to calculate the size distribution of the primary particles and their aggregates for each of the samples presented. SnSe itself (Figures 4c,f and S2 in the Supporting Information) is seen to be composed of approximately regular nanospheres with diameters in the range of  $7$ – $35\text{ nm}$  and that assemble into larger loose agglomerates. The morphology of the pristine ice-templated GO is entirely

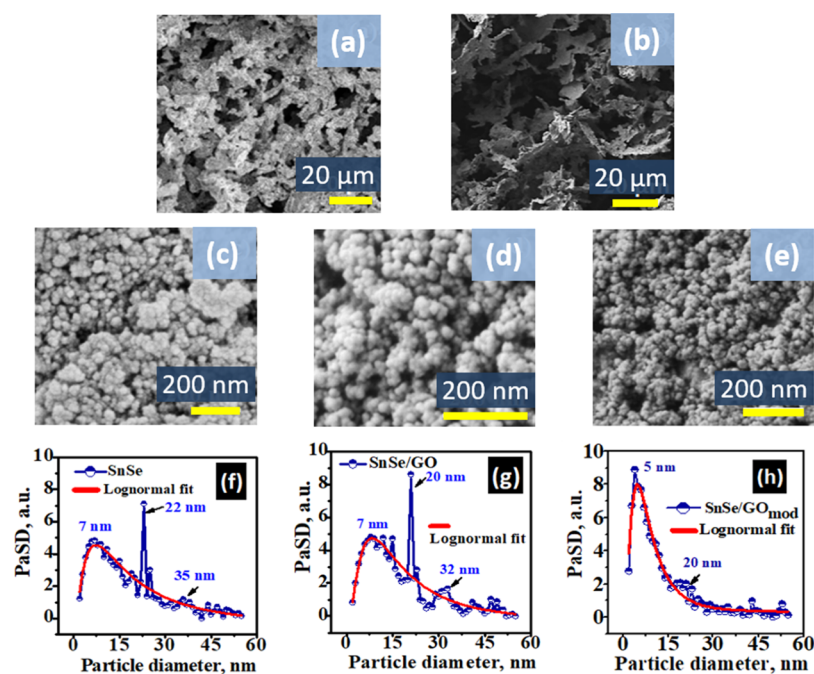


**Figure 4.** Low-magnification SEM images of (a) ice-templated SnSe/GO nanocomposite and (b) modified ice-templated SnSe/GO<sub>mod</sub> nanocomposite; high-magnification SEM images of (c) as-prepared SnSe, (d) ice-templated SnSe/GO nanocomposite, and (e) modified ice-templated SnSe/GO<sub>mod</sub> nanocomposite; (f–h) particle size distributions for SnSe, SnSe/GO, and SnSe/GO<sub>mod</sub> samples, respectively.

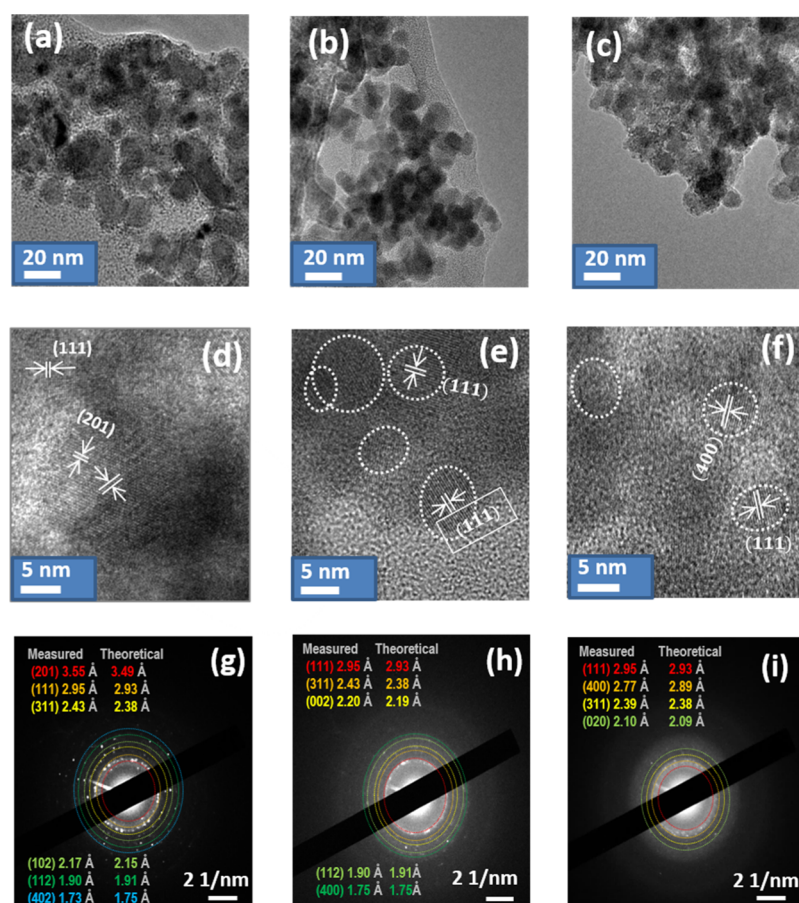


**Figure 5.** (a,d) HRTEM images of as-prepared SnSe nanoparticles and (g) corresponding SAED pattern indicating the polycrystalline nature of the SnSe nanoparticles; HRTEM images of ice-templated: (b,e) SnSe/GO and (c,f) SnSe/GO<sub>mod</sub> nanocomposites; SAED patterns of ice-templated: (h) SnSe/GO and (i) SnSe/GO<sub>mod</sub> nanocomposites.

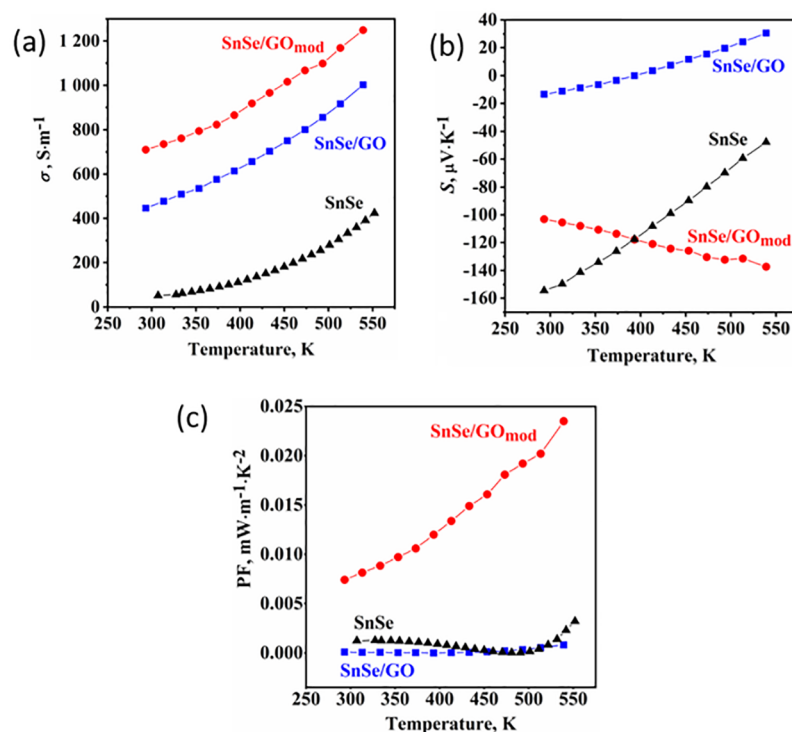


**Figure 6.** (a) Electrical conductivity, (b) the Seebeck coefficient, and (c) the power factor of neat SnSe, ice-templated SnSe/GO<sub>mod</sub>, and SnSe/GO nanocomposites.

different, and SEM images of the individual beads and their cross-sections indicate the distinctive porous structure with typical pore diameters of ca. 2–10  $\mu\text{m}$  (Figure S3). By comparison, lower magnification SEM images of both nanocomposites (Figures 4a,b, S4 and S5) indicate a mixing of sections of GO sheets with the SnSe nanoparticles creating a more porous microstructure than for SnSe itself (Figure 4c) but lacking the ordered macroporosity of pristine ice-templated GO (Figure S3). Looking at higher magnification (Figure 4d,e), the nanosphere-like morphology of SnSe itself is retained in the synthesized nanocomposites. The nanocomposite samples synthesized using unmodified GO (Figure 4d,g) were shown to form beads with diameters in a range that are slightly smaller (7–32 nm) than SnSe itself (Figure 4c,f). By contrast, the nanocomposites prepared using modified GO (Figure 4e,h) consist mostly of smaller nanoparticles dominated by those of a mean diameter of ca. 5 nm and to a lesser extent to particles 20 nm across. One would assume that the reduced nanoparticle size that predominates in the modified GO nanocomposites is a direct consequence of the GO surface modification, where the modifying agent that anchors to the GO surface likely acts in a similar fashion to a surfactant. In this case, the grafted silane chains can prevent the aggregation of nanoparticles by steric repulsion, thus hindering any further growth of the composite particles. The decrease in the GO<sub>mod</sub> particle size could be a promising development toward reducing the thermal conductivity via shortening the phonon mean free path and increasing the phonon scattering at the grain boundaries.<sup>50–54</sup> The high porosity indicated by the SEM images is also potentially beneficial as a means to increase phonon scattering centers as exemplified in systems such as Bi<sub>2</sub>Te<sub>3</sub>–PbTe where the porous microstructure exerts a significant positive influence on both the thermal conductivity and the value of the Seebeck

coefficient; careful control of these structural features can be exploited to improve the energy conversion efficiency of devices employing such materials.

TEM images and SAED patterns of neat SnSe and both nanocomposites are shown in Figure 5. The lattice fringes for neat SnSe can be clearly seen in HRTEM images (Figure 5d). Correspondingly, the measured interplanar distances  $d$  for various sets of lattice planes closely match with the expected planar separations for indexed planes from the orthorhombic phase of SnSe and SAED patterns could be successfully indexed on this basis (Figure 5g). For example, lattice spacings of 2.95 Å ( $d_{(111)}$ ) and 3.55 Å ( $d_{(201)}$ ) were typically observed in HRTEM images (Figure 5d). The diameter of the approximately spherical nanoparticles in the neat SnSe material was determined to be ca. 20–40 nm, which is in close agreement to estimates made from SEM images. It is observed from Figure 5b,c,e,f that the nanoparticles in the composites are typically a factor of 2 or more smaller than those of SnSe, again corroborating SEM results. It is difficult to discern separate (modified) GO sheets in the TEM images of the composites, which suggests a complete mixing of sheet fragments and SnSe. Both nanocomposites (Figure 5d,f) produce SAED patterns that are similar to those of as-synthesized SnSe, demonstrating that highly crystalline selenide particles are preserved within the nanocomposites; indeed, the measured interplanar distances are in excellent agreement with the expected  $d$ -spacings for orthorhombic SnSe.<sup>47,48</sup> It is also possible to note that in addition to the sharp diffraction spots associated with the orthorhombic SnSe phase, there are more diffuse rings which suggest the presence of (modified) GO, likely coating the SnSe particles. This is persuasive evidence that the (modified) GO has a role in preventing the agglomeration/growth of the SnSe particles (cf. Figure 5a).



Given that previous evidence has suggested that powders of SnSe lose mass above 600 K, thermal and electrical data were measured over a range from 290–540 K where the material is thermally stable.<sup>19</sup> As can be seen from Figure 6a, the electrical conductivity  $\sigma$  of the SnSe/GO<sub>mod</sub> nanocomposite increases from 708 S·m<sup>-1</sup> at 290 K to 1257 S·m<sup>-1</sup> at 539 K. It is especially notable that the values of the electrical conductivity obtained for the modified SnSe/GO<sub>mod</sub> nanocomposite are greater than those for both the unmodified SnSe/GO nanocomposite (increasing from 443 S·m<sup>-1</sup> at 290 K to 999 S·m<sup>-1</sup> at 539 K) and SnSe itself (conductivity increasing from ca. 55 S·m<sup>-1</sup> at 290 K to only 250 S·m<sup>-1</sup> at 539 K) over the same temperature range (Figure 6a), although the unmodified nanocomposites still compare well with some of the best previously reported SnSe nanomaterials.<sup>55</sup> Therefore, the effect of the GO component in the composites has some significance. That the conductivity of the unmodified composite is as high as observed is perhaps quite surprising given the electrically insulating nature of GO.<sup>56</sup> Less surprising perhaps is the fact that once many of the oxygen-containing functionalities have been removed by modification, the conductivity increases. In the context of electrical conductivity, the modified GO behaves more like reduced GO, graphene or indeed, “graphitic carbon nitride, g-C<sub>3</sub>N<sub>4</sub>” as a component in the modified composites.<sup>25</sup> (Interestingly there is evidence of C–N bonding by FTIR spectroscopy, as seen in Figure 1).

The contrast in the variation in the Seebeck coefficient  $S$  with temperature for each of the nanocomposites is stark (Figure 6b).  $S$  for SnSe/GO increases with temperature, showing the n-type behavior at room temperature and transforming to p-type behavior at 402 K with  $S \approx 31 \mu\text{V}\cdot\text{K}^{-1}$  at 539 K. By comparison,  $S$  for SnSe/GO<sub>mod</sub> has a negative sign—showing n-type behavior—across the entire measured temperature range and changes monotonically from  $-102 \mu\text{V}\cdot\text{K}^{-1}$  at room temperature to  $-136 \mu\text{V}\cdot\text{K}^{-1}$  at 539 K. Such behavior indicates that the majority charge carriers are electrons in both nanocomposites SnSe/GO and SnSe/GO<sub>mod</sub>. A comparison with the temperature-dependent behavior of  $S$  for SnSe itself, meanwhile, shows that the selenide itself exhibits n-type behavior at room temperature with a value of the coefficient that increases (becomes less negative) with increasing temperature, approaching a transition to p-type behavior at 539 K ( $S \approx -46 \mu\text{V}\cdot\text{K}^{-1}$ ). Given that n-type semiconductivity has been previously observed in SnSe nanoparticles prepared from hydrated SnCl<sub>2</sub>,<sup>55</sup> it would not be surprising if low levels of Cl<sup>-</sup> doping contributed to the negative Seebeck coefficients in both SnSe itself and the nanocomposites in our measurements. The notable difference in the magnitude of the coefficient in the modified SnSe/GO<sub>mod</sub> materials (and that the value remains negative with temperature, indeed becoming more negative as  $T$  increases), however, suggests an alternative (additional) source of electron doping, and this is consistent with the N-doping in the modified GO component (as indicated by spectroscopic data). Hence, the treatment with ODTs and TEA both increases the electrical conductivity and switches the semiconducting behavior from p-type (as observed in the majority of SnSe materials and at high  $T$  for the GO nanocomposite here) to n-type.

Taking the above electrical data and Seebeck values of neat SnSe and both nanocomposites, it was possible to derive values for the power factor,  $S^2\sigma$ , as a function of temperature (Figure 6c). A combination of high electrical conductivity coupled with

substantial (negative) values of the Seebeck coefficient,  $S$ , explains the significant difference in  $S^2\sigma$  for neat SnSe and unmodified composite as compared with modified one. The most important finding concerning the power factors of the two different types of nanocomposite and neat SnSe is that  $S^2\sigma$  for SnSe/GO<sub>mod</sub> is more than an order of magnitude (20-fold) higher than that for SnSe/GO nanocomposites and neat SnSe, at 539 K. The difference in power factor accomplished by the modification of the GO component is especially striking given that only 10 wt % of (modified) GO is used in the nanocomposites, and the effect is very similar to that engendered by doping SnSe with either iodine ( $S^2\sigma$  of  $\approx 0.016 \text{ mW m}^{-1} \text{ K}^{-2}$  at 565 K)<sup>6</sup> or chlorine ( $S^2\sigma$  of  $\approx 0.068 \text{ mW m}^{-1} \text{ K}^{-2}$  at 530 K).<sup>55</sup> It remains to be seen in future work as to what constitutes an optimum level of modified GO component for a high-performance SnSe/GO<sub>mod</sub> nanocomposite (or indeed whether alternative forms of functionalizing the GO can improve the transport properties still further). However, ultimately, it should prove beneficial to be able to replace at least some of the relatively expensive and environmentally detrimental raw materials (namely, tin, selenium, and halide additives where applicable) with ubiquitous carbon, nitrogen, and silicon. Coupled with the energy-efficient, aqueous solution synthesis approach used to prepare the SnSe component, there are thus several ways in which the introduction of SnSe-based materials could be made more sustainable.

Another obviously important criterion in assessing the effectiveness of a modified-GO composite approach to SnSe material development is an evaluation of the thermal transport behavior. At the present time, we have conducted preliminary thermal diffusivity measurements on hot pressed samples, given the challenges in accounting for the porosity of such materials and in representing their true experimental densities. By approximating the composite density as the sum of the components and making corrections for porosity,<sup>57</sup> we calculated the thermal conductivity (Figure S6) of the nanocomposites. It is perhaps not surprising that the total thermal conductivity of the unmodified SnSe/GO composite is lower than that of the modified material (by a factor of approximately 2; tentatively ca.  $0.4 \text{ W m}^{-1} \text{ K}^{-1}$  vs  $0.7 \text{ W m}^{-1} \text{ K}^{-1}$  at 550 K) given the likely more electrically and thermally insulating nature of GO compared to the SnSe/GO<sub>mod</sub> nanocomposite. Both nanocomposites exhibit values of  $\kappa_{\text{total}}$  of the same order as “pristine” solution-synthesized SnSe nanoparticles.<sup>58</sup> With further attenuation of the porosity and manipulation of GO functionalization/doping in association with advanced processing techniques such as spark plasma sintering, it should be possible to engineer nanocomposites with finely tuned electrical and thermal properties.

#### 4. CONCLUSIONS

This work demonstrates that it is possible to prepare ice-templated tin selenide-GO nanocomposites via a simple aqueous solution process. Moreover, it is possible to functionalize the GO component by way of modifying its surface using alkylamines. This allows the facile creation of both unmodified (SnSe/GO) and modified (SnSe/GO<sub>mod</sub>) composite materials for the first time. The chemical modification of the GO surface with TEA and ODTs produces significant changes to the electrical properties of the ensuing SnSe GO-based composites. Markedly, the surface-modified nanocomposite, SnSe/GO<sub>mod</sub>, exhibited higher electrical

conductivity and an increased negative Seebeck coefficient. The superior electrical conductivity and Seebeck coefficient give rise to  $S^2\sigma$  values that exceed those of typical as-prepared powders of SnSe. Further, the power factor for the modified SnSe/GO<sub>mod</sub> composite is 20 times that of the equivalent unmodified nanocomposite, SnSe/GO. Overall, these results suggest that freeze-cast GO nanocomposites formed with “active” thermoelectric components can provide a very effective means of influencing the electrical properties. Preliminary data suggest that thermal properties may be similarly tunable. The GO component in these nanocomposites affords a further layer of property and performance control via porosity and functionalization/modification of the surface. The approach should be adaptable to other material systems offering a new strategy for designing relatively inexpensive, lightweight, and low-toxicity thermoelectric materials and devices.

## ■ ASSOCIATED CONTENT

### ● Supporting Information

The Supporting Information is available free of charge on the ACS Publications website at DOI: 10.1021/acsomega.8b03146.

XRD patterns of both nanocomposites: (a) SnSe/GO and (b) SnSe/GO<sub>mod</sub> recorded after hot pressing; SEM image of parent SnSe at (a) higher and (b) lower magnification, EDS spectrum at a single point of (c) neat SnSe; SEM image of parent GO at (a) higher and (b) lower magnification; (a) SEM image of SnSe/GO nanocomposite, (b) EDS spectrum at a single point for SnSe/GO nanocomposite; SEM image of (a) SnSe/GO<sub>mod</sub> nanocomposite, (b) EDS spectrum at a single point of SnSe/GO<sub>mod</sub> nanocomposite; and thermal conductivity of modified SnSe/GO<sub>mod</sub> and unmodified SnSe/GO nanocomposites (PDF)

## ■ AUTHOR INFORMATION

### Corresponding Author

\*E-mail: [Duncan.Gregory@glasgow.ac.uk](mailto:Duncan.Gregory@glasgow.ac.uk).

### ORCID

Wuzong Zhou: 0000-0001-9752-7076

Jan-Willem G. Bos: 0000-0003-3947-2024

Yevhenii M. Morozov: 0000-0001-9689-8641

Duncan H. Gregory: 0000-0002-4585-3280

### Present Addresses

#College of Environment, Zhejiang University of Technology, Hangzhou 310014, China.

¶College of Science, Zhejiang University of Technology, Hangzhou 310023, China.

### Notes

The authors declare no competing financial interest.

## ■ ACKNOWLEDGMENTS

This work was financially supported by the EPSRC (EP/P510968/1). The authors thank Peter Chung for assistance with SEM. S.R.P. and J.W.G.B. acknowledge the EPSRC (grant EP/N01717X/1) for support.

## ■ ABBREVIATIONS

GO, graphene oxide; GO<sub>mod</sub>, modified graphene oxide; SnSe, tin selenide; TEA, triethylamine; ODTs, octadecyltriethox-

ysilane;  $\kappa$ , thermal conductivity;  $S^2\sigma$ , power factor;  $\sigma$ , electrical conductivity; EDS, energy-dispersive X-ray spectroscopy;  $S$ , Seebeck coefficient;  $T$ , temperature; IR, infrared spectroscopy; XRD, X-ray diffraction analysis; SEM, scanning electron microscopy; HRTEM, high resolution transmission electron microscopy; SAED, selected-area electron diffraction;  $ZT$ , figure of merit.

## ■ REFERENCES

- (1) Ding, G.; Gao, G.; Yao, K. High-efficient thermoelectric materials: The case of orthorhombic IV-VI compounds. *Sci. Rep.* **2015**, *5*, 9567.
- (2) Bell, L. E. Cooling, heating, generating power, and recovering waste heat with thermoelectric Systems. *Science* **2008**, *321*, 1457–1461.
- (3) Shi, X.; Yang, J.; Salvador, J. R.; Chi, M.; Cho, J. Y.; Wang, H.; Bai, S.; Yang, J.; Zhang, W.; Chen, L. Multiple-filled skutterudites: High thermoelectric figure of merit through separately optimizing electrical and thermal transports. *J. Am. Chem. Soc.* **2011**, *133*, 7837–7846.
- (4) Zhao, L.-D.; Lo, S.-H.; Zhang, Y.; Sun, H.; Tan, G.; Uher, C.; Wolverton, C.; Dravid, V. P.; Kanatzidis, M. G. Ultralow thermal conductivity and high thermoelectric figure of merit in SnSe crystals. *Nature* **2014**, *508*, 373–377.
- (5) Chen, C.-L.; Wang, H.; Chen, Y.-Y.; Day, T.; Snyder, G. J. Thermoelectric properties of p-type polycrystalline SnSe doped with Ag. *J. Mater. Chem. A* **2014**, *2*, 11171–11176.
- (6) Zhang, Q.; Chere, E. K.; Sun, J.; Cao, F.; Dahal, K.; Chen, S.; Chen, G.; Ren, Z. Studies on Thermoelectric properties of n-type polycrystalline SnSe<sub>1-x</sub>S<sub>x</sub> by iodine doping. *Adv. Energy Mater.* **2015**, *5*, 1500360.
- (7) Sassi, S.; Candolfi, C.; Vaney, J.-B.; Ohorodniichuk, V.; Masschelein, P.; Dauscher, A.; Lenoir, B. Assessment of the thermoelectric performance of polycrystalline p-type SnSe. *Appl. Phys. Lett.* **2014**, *104*, 212105.
- (8) Carrete, J.; Mingo, N.; Curtarolo, S. Low thermal conductivity and triaxial phononic anisotropy of SnSe. *Appl. Phys. Lett.* **2014**, *105*, 101907.
- (9) Zhang, H.; Talapin, D. V. Thermoelectric tin selenide: The beauty of simplicity. *Angew. Chem., Int. Ed. Engl.* **2014**, *53*, 9126–9127.
- (10) Han, C.; Sun, Q.; Li, Z.; Dou, S. X. Thermoelectric enhancement of different Kinds of metal chalcogenides. *Adv. Energy Mater.* **2016**, *6*, 1600498.
- (11) Lee, Y. K.; Ahn, K.; Cha, J.; Zhou, C.; Kim, H. S.; Choi, G.; Chae, S. I.; Park, J.-H.; Cho, S.-P.; Park, S. H.; Sung, Y.-E.; Lee, W. B.; Hyeon, T.; Chung, I. Enhancing p-Type Thermoelectric Performances of Polycrystalline SnSe via Tuning Phase Transition Temperature. *J. Am. Chem. Soc.* **2017**, *139*, 10887–10896.
- (12) Sassi, S.; Candolfi, C.; Vaney, J.-B.; Ohorodniichuk, V.; Masschelein, P.; Dauscher, A.; Lenoir, B. Assessment of the thermoelectric performance of polycrystalline p-type SnSe. *Appl. Phys. Lett.* **2014**, *104*, 212105.
- (13) Singh, N. K.; Bathula, S.; Gahtori, B.; Tyagi, K.; Haranath, D.; Dhar, A. The effect of doping on thermoelectric performance of p-type SnSe: Promising thermoelectric material. *J. Alloys Compd.* **2016**, *668*, 152–158.
- (14) Wubieneh, T. A.; Chen, C.-L.; Wei, P. C.; Chen, S.-Y.; Chen, Y.-Y. The effects of Ge doping on the thermoelectric performance of p-type polycrystalline SnSe. *RSC Adv.* **2016**, *6*, 114825–114829.
- (15) Liu, J.; Wang, P.; Wang, M.; Xu, R.; Zhang, J.; Liu, J.; Li, D.; Liang, N.; Du, Y.; Chen, G.; Tang, G. Achieving High Thermoelectric Performance with Pb and Zn Codoped Polycrystalline SnSe via Phase Separation and Nanostructuring Strategies. *Nano Energy* **2018**, *53*, 683–689.
- (16) Chandra, S.; Banik, A.; Biswas, K. n-Type Ultrathin few-layer nanosheets of Bi-doped SnSe: Synthesis and thermoelectric properties. *ACS Energy Lett.* **2018**, *3*, 1153–1158.



- (17) Li, F.; Wang, W.; Qiu, X.; Zheng, Z.; Fan, P.; Luo, J.; Li, B. Optimization of thermoelectric properties of n-type Ti, Pb co-doped SnSe. *Inorg. Chem. Front.* **2017**, *4*, 1721–1729.
- (18) (a) Chang, C.; Tan, Q.; Pei, Y.; Xiao, Y.; Zhang, X.; Chen, Y.-X.; Zheng, L.; Gong, S.; Li, J.-F.; He, J.; Zhao, L.-D. Raising thermoelectric performance of n-type SnSe via Br doping and Pb alloying. *RSC Adv.* **2016**, *6*, 98216–98220. (b) Shi, X.-L.; Zheng, K.; Liu, W.-D.; Wang, Y.; Yang, Y.-Z.; Chen, Z.-G.; Zou, J. Realizing high thermoelectric performance in n-type highly distorted Sb-doped SnSe microplates via tuning high electron concentration and inducing intensive crystal defects. *Adv. Energy Mater.* **2018**, *8*, 1800775.
- (19) Han, G.; Popuri, S. R.; Greer, H. F.; Bos, J.-W. G.; Zhou, W.; Knox, A. R.; Montecucco, A.; Siviter, J.; Man, E. A.; Macauley, M.; Paul, D. J.; Li, W.-G.; Paul, M. C.; Gao, M.; Sweet, T.; Freer, R.; Azough, F.; Baig, H.; Sellami, N.; Mallick, T. K.; Gregory, D. H. Facile surfactant-free synthesis of p-type SnSe nanoplates with exceptional thermoelectric power factors. *Angew. Chem., Int. Ed. Engl.* **2016**, *55*, 6433–6437.
- (20) Novoselov, K. S.; Geim, A. K.; Morozov, S. V.; Jiang, D.; Zhang, Y.; Dubonos, S. V.; Grigorieva, I. V.; Firsov, A. A. Electric field effect in atomically thin carbon films. *Science* **2004**, *306*, 666–669.
- (21) Pierson, H. O. *Handbook of Carbon, Graphite, Diamond And Fullerenes: Properties, Processing And Applications*; Noyes Publications: Park Ridge, NJ, 1993.
- (22) Dollfus, P.; Hung Nguyen, V.; Saint-Martin, J. Thermoelectric effects in graphene nanostructures. *J. Phys.: Condens. Matter* **2015**, *27*, 133204.
- (23) Zhou, S.; Guo, Y.; Zhao, J. Enhanced thermoelectric properties of graphene oxide patterned by nanoroads. *Phys. Chem. Chem. Phys.* **2016**, *18*, 10607–10615.
- (24) Maharubin, S.; Zhang, X.; Zhu, F.; Zhang, H.-C.; Zhang, G.; Zhang, Y. Synthesis and applications of semiconducting graphene. *J. Nanomater.* **2016**, *2016*, 1–19.
- (25) Dong, J.; Liu, W.; Li, H.; Su, X.; Tang, X.; Uher, C. In situ synthesis and thermoelectric properties of PbTe-graphene nanocomposites by utilizing a facile and novel wet chemical method. *J. Mater. Chem. A* **2013**, *1*, 12503–12511.
- (26) Zong, P.-a.; Hanus, R.; Dylla, M.; Tang, Y.; Liao, J.; Zhang, Q.; Snyder, G. J.; Chen, L. Skutterudite with graphene-modified grain-boundary complexation enhances zT enabling high-efficiency thermoelectric device. *Energy Environ. Sci.* **2017**, *10*, 183–191.
- (27) Ahmad, K.; Wan, C.; Al-Eshaikh, M. A.; Kadachi, N. Enhanced thermoelectric performance of Bi<sub>2</sub>Te<sub>3</sub> based graphene nanocomposites. *Appl. Surf. Sci.* **2018**, *474*, 2.
- (28) Qiao, H.; Huang, Z.; Ren, X.; Yao, H.; Luo, S.; Tang, P.; Qi, X.; Zhong, J. Photoresponse improvement in liquid-exfoliated SnSe nanosheets by reduced graphene oxide hybridization. *J. Mater. Sci.* **2018**, *53*, 4371–4377.
- (29) Yao, H.; Luo, S.; Duesberg, G. S.; Qi, X.; Lu, D.; Yue, C.; Zhong, J. Enhanced photoresponse of graphene oxide functionalised SnSe films. *AIP Adv.* **2018**, *8*, 075123.
- (30) Shiravizadeh, A. G.; Yousefi, R.; Elahi, S. M.; Sebt, S. A. Effects of annealing atmosphere and rGO concentration on the optical properties and enhanced photocatalytic performance of SnSe/rGO nanocomposites. *Phys. Chem. Chem. Phys.* **2017**, *19*, 18089–18098.
- (31) Yang, X.; Zhang, R.; Chen, N.; Meng, X.; Yang, P.; Wang, C.; Zhang, Y.; Wei, Y.; Chen, G.; Du, F. Assembly of SnSe nanoparticles confined in graphene for enhanced sodium-ion storage performance. *Chem.—Eur. J.* **2016**, *22*, 1445–1451.
- (32) Yu, H.; Zhang, B.; Bulin, C.; Li, R.; Xing, R. High-efficient synthesis of graphene oxide based on improved hummers method. *Sci. Rep.* **2016**, *6*, 36143.
- (33) Marcano, D. C.; Kosynkin, D. V.; Berlin, J. M.; Sinitskii, A.; Sun, Z.; Slesarev, A.; Alemany, L. B.; Lu, W.; Tour, J. M. Improved synthesis of graphene oxide. *ACS Nano* **2010**, *4*, 4806–4814.
- (34) (a) Godula-Jopek, A.; Gregory, D. H.; Champet, S.; Westenberger, A.; Warmuzinski, K. Ammonia borane confinement in graphene oxide 3d structures, U.S. Patent 20,180,194,622 A1, 2018. (b) Champet, S.; van den Berg, J.; Szczesny, R.; Godula-Jopek, A.; Gregory, D. H. Nano-inclusion in One Step: Spontaneous ice-templating of porous hierarchical nanocomposites for selective hydrogen release. *Sustainable Energy Fuels* **2019**, *3*, 396–400.
- (35) Matsuo, Y.; Fukunaga, T.; Fukutsuka, T.; Sugie, Y. Silylation of graphite oxide. *Carbon* **2004**, *42*, 2117–2119.
- (36) Asakura, Y.; Sakamoto, Y.; Kuroda, K. Silylation of layered silicate RUB-51 with SiCl<sub>4</sub> and conversion of the silylated derivative to a crystalline microporous material. *Chem. Mater.* **2014**, *26*, 3796–3803.
- (37) Takahashi, N.; Kuroda, K. Chemical modification of interlayer surfaces of layered silicates and transformation to nanostructured materials. *J. Mater. Chem.* **2011**, *21*, 14336.
- (38) Deville, S.; Meille, S.; Seuba, J. A meta-analysis of the mechanical properties of ice-templated ceramics and metals. *Sci. Technol. Adv. Mater.* **2015**, *16*, 043501.
- (39) Lerf, A.; He, H.; Forster, M.; Klinowski, J. Structure of graphite oxide revisited. *J. Phys. Chem. B* **1998**, *102*, 4477–4482.
- (40) Ferrari, A. C.; Robertson, J. Raman spectroscopy of amorphous, nanostructured, diamond-like carbon, and nanodiamond. *Philos. Trans. R. Soc., A* **2004**, *362*, 2477–2512.
- (41) Zhao, J.; Liu, L.; Li, F. *Graphene oxide: physics and applications*; Springer: Heidelberg, 2015.
- (42) Saritha, K.; Phaneendra Reddy, G.; Ramakrishna Reddy, K. T. Studies on physical properties of SnSe<sub>2</sub> thin films grown by a two-stage process. *Mater. Today* **2016**, *3*, 4128–4133.
- (43) Posudievsky, O. Y.; Khazieieva, O. A.; Koshechko, V. G.; Pokhodenko, V. D. Preparation of graphene oxide by solvent-free mechanochemical oxidation of graphite. *J. Mater. Chem.* **2012**, *22*, 12465.
- (44) Campos-Delgado, J.; Romo-Herrera, J. M.; Jia, X.; Cullen, D. A.; Muramatsu, H.; Kim, Y. A.; Hayashi, T.; Ren, Z.; Smith, D. J.; Okuno, Y.; Ohba, T.; Kanoh, H.; Kaneko, K.; Endo, M.; Terrones, H.; Dresselhaus, M. S.; Terrones, M. Bulk production of a new form of sp<sup>2</sup> carbon: crystalline graphene nanoribbons. *Nano Lett.* **2008**, *8*, 2773–2778.
- (45) Thangappan, R.; Kalaiselvam, S.; Elayaperumal, A.; Jayavel, R. Synthesis of graphene oxide/vanadium pentoxide composite nanofibers by electrospinning for supercapacitor applications. *Solid State Ionics* **2014**, *268*, 321–325.
- (46) Bernardes-Silva, A. C.; Mesquita, A. F.; Neto, E. d. M.; Porto, A. O.; Ardisson, J. D. XRD and <sup>119</sup>Sn Mössbauer spectroscopy characterization of SnSe obtained from a simple chemical route. *Mater. Res. Bull.* **2005**, *40*, 1497–1505.
- (47) Wiedemeier, H.; von Schnering, H. G. Refinement of the structures of GeS, GeSe, SnS and SnSe. *Z. Kristallogr.* **1978**, *148*, 295–303.
- (48) Chattopadhyay, T.; Pannetier, J.; Von Schnering, H. G. Neutron diffraction study of the structural phase transition in SnS and SnSe. *J. Phys. Chem. Solids* **1986**, *47*, 879–885.
- (49) Devaux, M. F.; Legland, D. Grey level granulometry for histological image analysis of plant tissues. In *Microscopy: advances in scientific research and education*; Méndez-Vilas, A., Ed.; Formatex Research Center: Badajoz, Spain, 2014; Vol. 2, pp 681–688.
- (50) Zuev, Y. M.; Lee, J. S.; Galloy, C.; Park, H.; Kim, P. Diameter dependence of the transport properties of antimony telluride nanowires. *Nano Lett.* **2010**, *10*, 3037–3040.
- (51) Ohta, H.; Kim, S.; Mune, Y.; Mizoguchi, T.; Nomura, K.; Ohta, S.; Nomura, T.; Nakanishi, Y. Giant thermoelectric Seebeck coefficient of two-dimensional electron gas in SrTiO<sub>3</sub>. *Nat. Mater.* **2007**, *6*, 129–134.
- (52) Koumoto, R. Y.; Feser, J. P.; Lee, J.-S.; Talapin, D. V.; Segalman, R.; Majumdar, A. Enhanced thermopower in PbSe nanocrystal quantum dot superlattices. *Nano Lett.* **2008**, *8*, 2283–2288.
- (53) Boukai, A. I.; Bunimovich, Y.; Tahir-Kheli, J.; Yu, J.-K.; Goddard, W. A., III; Heath, J. R. Silicon nanowires as efficient thermoelectric materials. *Nature* **2008**, *451*, 168–171.
- (54) Yoon, S.; Kwon, O.-J.; Ahn, S.; Kim, J.-Y.; Koo, H.; Bae, S.-H.; Cho, J.-Y.; Kim, J.-S.; Park, C. The effect of grain size and density on

the thermoelectric properties of Bi<sub>2</sub>Te<sub>3</sub>-PbTe compounds. *J. Electron. Mater.* **2013**, *42*, 3390–3396.

(55) Han, G.; Popuri, S. R.; Greer, H. F.; Llin, L. F.; Bos, J.-W. G.; Zhou, W.; Paul, D. J.; Ménard, H.; Knox, A. R.; Montecucco, A.; Siviter, J.; Man, E. A.; Li, W.-G.; Paul, M. C.; Gao, M.; Sweet, T.; Freer, R.; Azough, F.; Baig, H.; Mallick, T. K.; Gregory, D. H. Chlorine-enabled electron doping in solution-synthesized SnSe thermoelectric nanomaterials. *Adv. Energy Mater.* **2017**, *7*, 1602328.

(56) Dreyer, D. R.; Park, S.; Bielawski, C. W.; Ruoff, R. S. The chemistry of graphene oxide. *Chem. Soc. Rev.* **2010**, *39*, 228–240.

(57) Xu, B.; Feng, T.; Agne, M. T.; Zhou, L.; Ruan, X.; Snyder, G. J.; Wu, Y. Highly Porous Thermoelectric Nanocomposites with Low Thermal Conductivity and High Figure of Merit from Large-Scale Solution-Synthesized Bi<sub>2</sub>Te<sub>2.5</sub>Se<sub>0.5</sub> Hollow Nanostructures. *Angew. Chem., Int. Ed.* **2017**, *56*, 3546–3551.

(58) Han, G.; Popuri, S. R.; Greer, H. F.; Zhang, R.; Ferre-Llin, L.; Bos, J.-W. G.; Zhou, W.; Reece, M. J.; Paul, D. J.; Knox, A. R.; Gregory, D. H. Topotactic anion-exchange in thermoelectric nanostructured layered tin chalcogenides with reduced selenium content. *Chem. Sci.* **2018**, *9*, 3828–3836.